

Article

# Removal Mechanism of Mineral Impurities in Molybdenum Concentrate Treatment Process

Qihang Liu <sup>1,2,3,\*</sup>, Ruilin Liu <sup>1</sup>, Shuangping Yang <sup>1,2</sup>, Weiguo Feng <sup>3</sup> and Miao Wang <sup>1,2</sup><sup>1</sup> School of Metallurgical Engineering, Xi'an University of Architecture and Technology, Xi'an 710055, China<sup>2</sup> Metallurgical Engineering Technology Research Center of Shaanxi Province, Xi'an 710055, China<sup>3</sup> Technical Centre, Jinduicheng Molybdenum Co., Ltd., Xi'an 710077, China

\* Correspondence: liuqh@xauat.edu.cn

**Abstract:** The removal of impurities in molybdenum concentrate has become a new challenge for enterprises due to the cancellation of pickling. Whether impurity minerals can be converted into soluble ions during roasting is important for the impurity removal by current water washing. In this work, the interaction between various impurity elements in the treatment process of molybdenum concentrate was studied by process simulation experiments combined with X-ray fluorescence (XRF) and X-ray diffraction (XRD), inductively coupled plasma-optical emission spectrometer (ICP-OES), ion chromatography (IC), scanning electron microscope-energy dispersive spectrometry (SEM-EDS), the use of FactSage7.0 modeling and the mineral liberation analyzer (MLA). The results show that most of the impurity elements such as K, Si and Al exist in the form of alkaline minerals with large molecular weight. In the roasting process of molybdenum concentrate, K-containing minerals, such as muscovite and orthoclase, can be transformed into  $K^+$ ,  $Al^{3+}$  and other soluble ions, and then can be removed by water washing. Humidification increased the conversion degree of orthoclase to soluble ions, which was conducive to the removal of impurities by the washing process. The results of MLA microscopic analysis confirmed that impurities such as  $FeS_2$ ,  $CaSO_4$ ,  $SiO_2$ , and especially  $FeS_2$ , would form a high density mixture with  $MoO_3$  during the high temperature roasting process, and thus reduced the leaching rate of Mo. Therefore, the humidification and control of the molybdenum concentrate is an effective measure to remove impurities.

**Keywords:** impurity removal; molybdenum concentrate; thermodynamic; roasting; humidification

**Citation:** Liu, Q.; Liu, R.; Yang, S.; Feng, W.; Wang, M. Removal Mechanism of Mineral Impurities in Molybdenum Concentrate Treatment Process. *Minerals* **2023**, *13*, 35. <https://doi.org/10.3390/min13010035>

Academic Editor: Chiharu Tokoro

Received: 26 October 2022

Revised: 23 December 2022

Accepted: 23 December 2022

Published: 26 December 2022



**Copyright:** © 2022 by the authors. Licensee MDPI, Basel, Switzerland. This article is an open access article distributed under the terms and conditions of the Creative Commons Attribution (CC BY) license (<https://creativecommons.org/licenses/by/4.0/>).

## 1. Introduction

Molybdenum is a metal with a high melting point, high wear resistance and good electrical and thermal conductivity, which is widely used in alloys, electrodes, catalysts, composite materials and other fields [1,2]. Impurity elements such as K, Si and Al have a serious impact on the quality of molybdenum products. In recent years, enterprises have paid more and more attentions to the content of impurities, especially K, in molybdenum products. When the potassium content of industrial grade molybdenum trioxide exceeds 1000–1500 mg/kg, it is unsuitable for use in special raw materials such as catalysts and reducing agents for petrochemical and organic synthesis. It is also ineffective for making alkaloid reagents and organic synthesis intermediates directly [3–5]. Under high temperature and high pressure, potassium impurities in the target material of very large scale integration circuit (VLSI) and liquid crystal display (LCD) are easily broken down and become defective pixels, affecting their service life [6–9].

The actual production process showed that in ammonium molybdate solution with molybdenum content greater than 250 g/L, the quality of ammonium molybdate produced by controlling potassium content to less than 60 mg/L was basically acceptable, but potassium content in actual production was usually more than 100 mg/L [10–13]. In addition, Ca, Fe, Si, Na and other impurity elements also affect the extraction of Mo and

the content of K in the product during ammonium molybdate production. Therefore, it is necessary to study the thermodynamic behavior and solubility changes of typical impurity elements during ammonium molybdate production.

Pickling molybdenum calcine can effectively remove impurity elements such as K, Si, Na etc., however the pickling liquid leads to Mo loss and is difficult to treat to prevent it from causing environmental harm. Using this method to remove impurities in production is currently prohibited in China [14–16]. Presently, the major method for removing impurity elements during ammonium molybdate manufacturing is to wash calcined molybdenum concentrate with water; this approach is good for the removal of soluble ions. Production showed that impurities, especially K, in the ammonium molybdate product were mainly released from the water-insoluble potassium minerals [17]. Therefore, being able to convert impurity elements into water-soluble ionic forms in the roasting process is very important for the production of low potassium and high purity molybdenum products [18–22].

Wang et al. [23] studied the effect of impurity elements such as Ca, Fe, Al, etc., on the sintering phenomenon of molybdenum concentrate during the roasting process. In order to improve the quality of molybdenite, Tumen-Ulzii et al. [24] studied the selective dissolution of copper and iron by acidic sodium nitrate for molybdenite concentrate containing chalcopyrite and pyrite leached. Wang et al. [25] proposed that the agglomeration of molybdenite is often accompanied by caking in the process of oxidation roasting, and reducing the content of impurity elements such as Fe can effectively reduce the occurrence of agglomeration. However, there is still no report on whether particle size affects the removal of impurity elements or the Mo extraction. In addition, traditional methods such as X-ray diffraction (XRD), scanning electron microscope-energy dispersive spectrometer (SEM-EDS), X-ray photoelectron spectroscopy (XPS) etc., have been used in most studies to analyze the effect of impurity elements on the Mo leaching process [26]. The impurity elements mostly exist in the form of minerals such as muscovite, orthoclase, pyrite, quartz, etc. This is actually not completely consistent with the geological survey results of molybdenum ore, mainly because the content of potassium minerals in molybdenum concentrate is very low ( $10^{-3}$ ~ $10^{-5}$ ), which cannot be quantitatively analyzed by these analytical methods. Therefore, more advanced analytical methods are needed to analyze the transformation mechanism of impurity minerals.

Mineral liberation analyzer (MLA) technology, which contains a high-speed automatic mineral parameter analysis system, is mainly used for the quantitative analysis of phases in geoscience, mining and other fields [27]. There is no report on the application of MLA technology to the analysis of impurity minerals in the production process of ammonium molybdate. Based on the combination of advanced MLA quantitative analysis results and the Factsage software, this work analyzes the interaction and thermodynamic behavior of impurity elements in the roasting process of molybdenum concentrate. The results provide theoretical support for the production of low potassium and high purity molybdenum products.

## 2. Experimental Method

### 2.1. Experiment of Roasting-Water Washing-Ammonia Leaching

The molybdenum concentrate used in this experiment came from a molybdenum processing enterprise in Shaanxi, China. Molybdenum concentrate with different particle sizes was processed by simulating the production process of ammonium molybdate (as shown in Figure 1). The molybdenum concentrate was screened at 48  $\mu\text{m}$ , 75  $\mu\text{m}$  and 106  $\mu\text{m}$ . The screened molybdenum concentrate was divided into coarse molybdenum concentrate with size range 75~106  $\mu\text{m}$  and fine molybdenum concentrate with size range 48~75  $\mu\text{m}$ . Unscreened molybdenum concentrate, coarse molybdenum concentrate and fine molybdenum concentrate of the same mass (100 g) were each roasted in a tube furnace with atmosphere control.

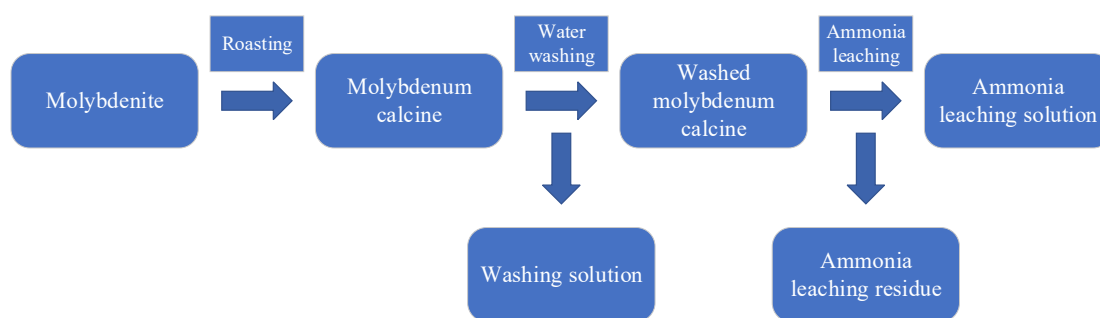


**Figure 1.** Ammonium molybdate production process.

The heating rate was controlled at 10 °C/min in the simulation of the actual production process. When the temperature reached 580 °C, it was kept for 4 h. After roasting, the calcined samples were cooled by natural cooling. Then, the samples were soaked in distilled water with liquid-solid ratio of 5:4 at room temperature for 1 h. After that, the samples were collected on filter paper, and put into the electric blast air constant temperature drying oven at 110 °C for 4 h. Finally, the ammonia leaching experiment was carried out on the dried molybdenum calcine. Samples were taken from each of the dried products and placed into beakers. Ammonia solution with a concentration of 28% (*w/w*) was added with a liquid-solid ratio of 3:1, and the ammonia leaching residue was filtered after soaking for 250 min. The mass of samples before and after roasting, washing and ammonia leaching was recorded.

The experiment to examine humidification of molybdenum concentrate during roasting was also carried out in a tube furnace. The molybdenum concentrate sample was heated at the rate of 10 °C/min; when the temperature reached 580 °C, it was kept for 3.5 h. Then the roasting temperature was set to 500 °C, water vapor and air were mixed in a ratio of 1:2 and passed into the tube furnace. Finally, the samples were slowly cooled and removed to be soaked in 200 mL deionized water for 5 h and then filtered and dried. After drying, the contents of impurity elements and compounds were determined by X-ray fluorescence spectrometry (XRF: ZSX100e, Rigaku Corporation, Akishima-shi, Japan) and mineral liberation analyser (MLA, Bruker, Massachusetts, The United States of America).

### 2.2. Chemical Composition Analysis of Different Products

10 g of the molybdenum concentrate, molybdenum calcine, washed molybdenum calcine and ammonia leaching residue produced as described in Section 2.1 were taken and ground in a mortar to pass 75 µm. The ion contents of these samples were determined by inductively coupled plasma-optical emission spectrometry (ICP-OES: Agilent 5110, Agilent Technologies Inc., Santa Clara, CA, USA), ion chromatography (IC: ICS-1100, DIONEX, Sunnyvale, CA, USA) and the chemical composition was analyzed by X-ray fluorescence spectrometry (XRF: ZSX100e, Rigaku Corporation, Akishima-shi, Japan).

### 2.3. Phase Analysis of Different Products

The phases present in the product samples were analyzed by XRD (X'Pert Pro MPD, PANalytical B.V., Heracles Almelo, Almelo, The Netherlands), SEM-EDS (JSM-5610LV, JEOL, Akishima-shi, Japan) and mineral liberation analyzer (MLA, Bruker, MA, USA). The working distance of SEM-EDS was 4.94 µm, the test magnification was 10 kx, the measurement was 10 µm, the voltage was 10 keV, and the field of view was 12.7 µm. The MLA system was composed of scanning electron microscope (Sigma 300, Carl Zeiss AG, Oberkochen, Germany), Bruker's energy spectrometer (Quantax 400, Bruker, Massachusetts, The United States of America) and Bruker's AMICS mineral analysis software (ESPRIT 1.9). The test temperature was 24 °C, the voltage was 20 kV, and the scanning resolution was 1.12 µm.

### 3. Results and Discussion

#### 3.1. Main Elements in Molybdenum Concentrates with Different Particle Sizes

From the screening of concentrate as described in Section 2.1, the weight of finer molybdenum concentrates from 48  $\mu\text{m}$  to 75  $\mu\text{m}$  accounts for about 70% of the material in the 48  $\mu\text{m}$  to 106  $\mu\text{m}$  range. The contents of the main elements in the two samples are shown in Figure 2.

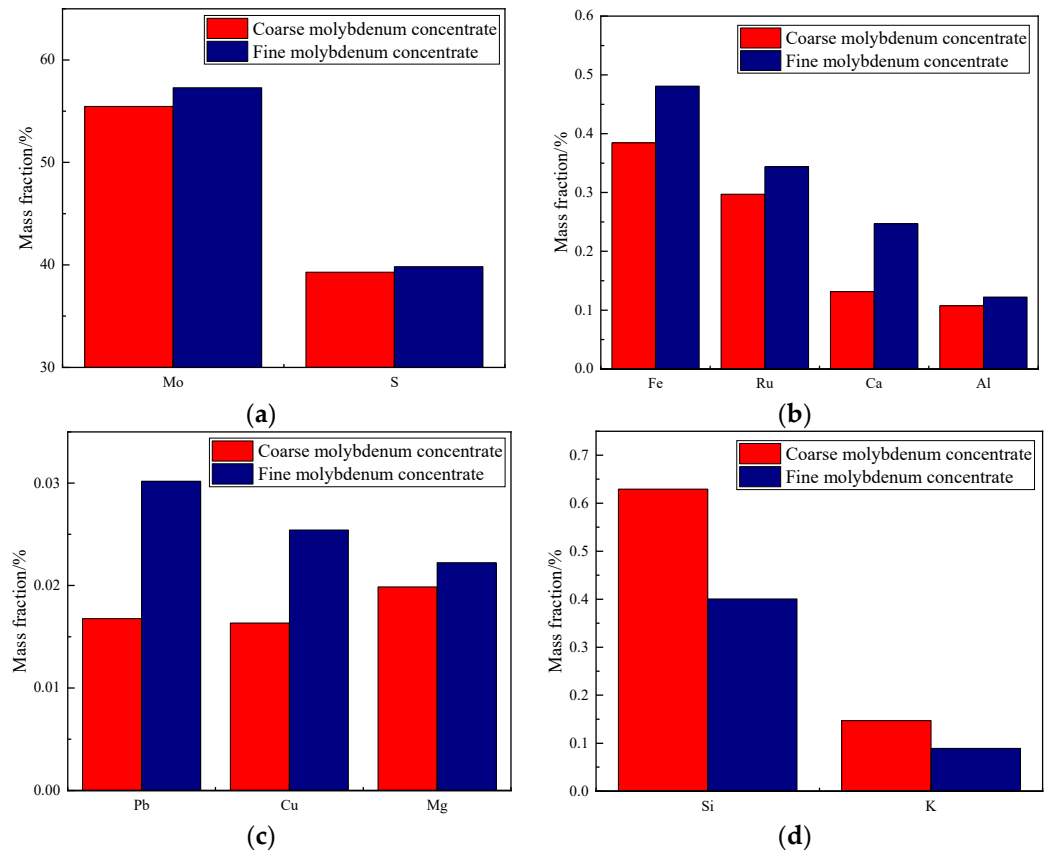


**Figure 2.** Distribution of elements in molybdenum concentrates with different particle sizes. (a) Content of Mo, S; (b) Content of Fe, Ru, Ca, Al; (c) Content of Pb, Cu, Mg; (d) Content of Si, K.

The main component of molybdenum concentrate is  $\text{MoS}_2$ . According to the mass fraction of molybdenum and sulfur in Figure 2, it can be seen that the ratio of sulfur is still surplus after  $\text{MoS}_2$  is fully proportioned with molybdenum, which suggests the presence of other sulfur-containing minerals. It can also be seen from Figure 2 that  $\text{MoS}_2$  in molybdenum concentrate mainly exists in the finer particle size fraction, and metal impurities in fine molybdenum concentrate are significantly more, while potassium and silicon contents in coarse molybdenum concentrate are slightly higher than those in fine molybdenum concentrate.

#### 3.2. Speciation and Phase Analysis of Impurity Elements

XRD analysis results for the whole molybdenum concentrate and molybdenum calcine samples are shown in Figure 3.

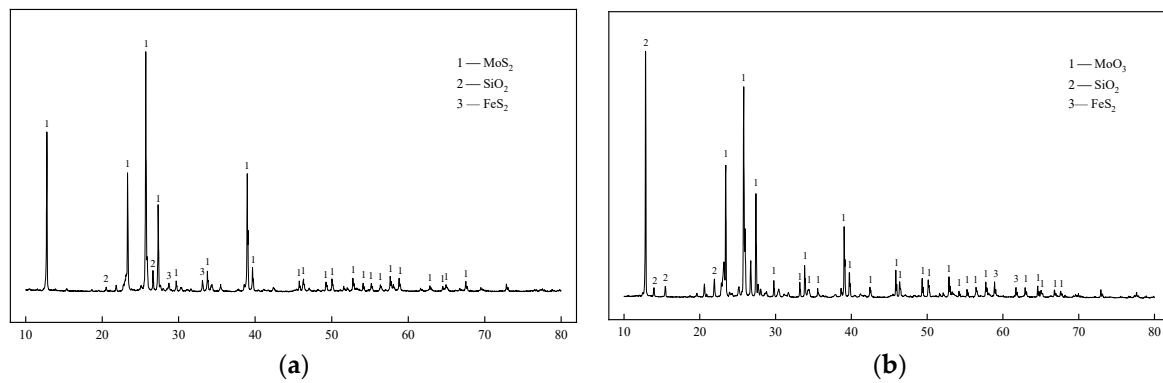


**Figure 3.** XRD analysis of molybdenum concentrate and molybdenum calcine. (a) molybdenum concentrate; (b) molybdenum calcine.

According to the XRD results in Figure 3a,  $\text{MoS}_2$  is the primary component of molybdenum concentrate, and the diffraction peaks of other impurities are not visible due to their low contents, leaving only  $\text{SiO}_2$  and  $\text{FeS}_2$ . After oxidative roasting, the main component  $\text{MoS}_2$  in the molybdenum concentrate is oxidized to  $\text{MoO}_3$  as shown in Figure 3b.

The main elements in the whole molybdenum concentrate, and its molybdenum calcine and ammonia leaching residue were analyzed by SEM-EDS. The semi-quantitative analysis results of different impurity elements can be obtained by SEM-EDS as shown in Figure 4 and Table 1. (Scatter plot 1, 2 and 3 are matched with the samples of molybdenum concentrate, molybdenum calcine and ammonia leaching residue, respectively).

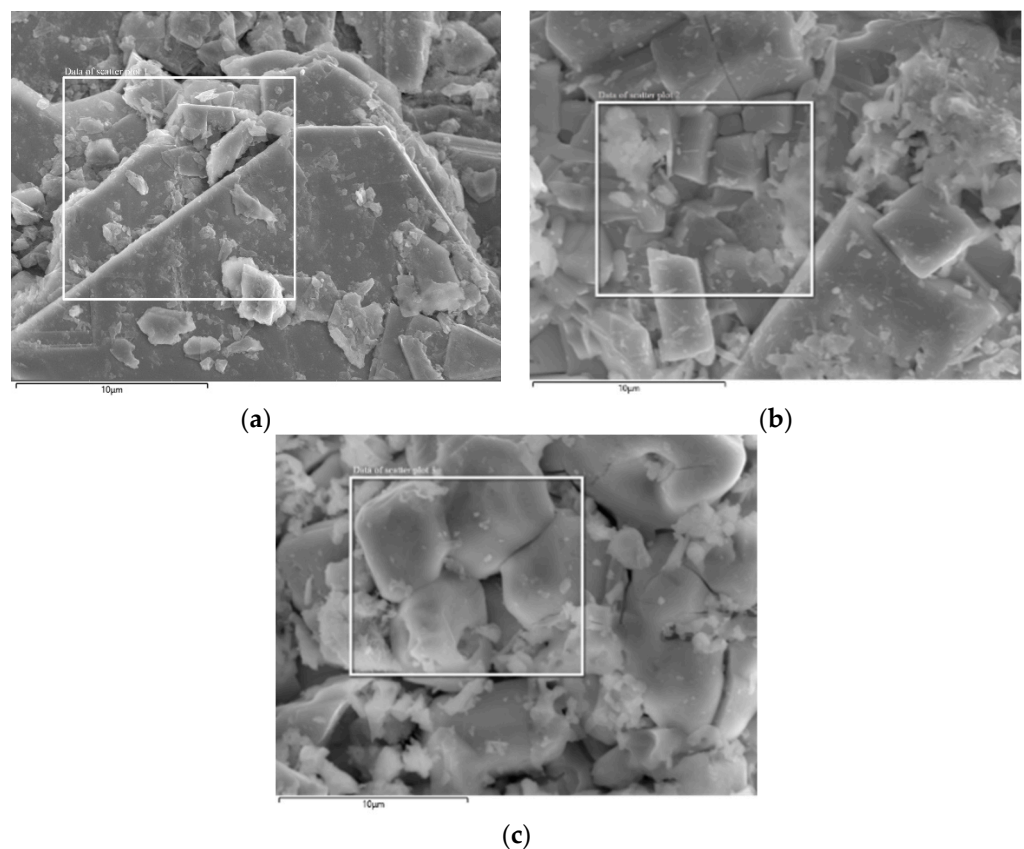


**Figure 4.** SEM images of different samples. (a) Molybdenum concentrate; (b) Molybdenum calcine; (c) Ammonia leaching residue.

**Table 1.** EDS analysis of main elements in different samples/%.

Element	Molybdenum Concentrate	Molybdenum Calcine	Ammonia Leaching Residue
O	1.49	40.54	41.49
Al	0.13	0.14	2.79
S	40.67	1.07	0.86
K	0.13	0.15	0.08
Fe	0.46	0.48	20.17
Mo	56.44	56.91	12.24
Si	0.68	0.71	22.37

Table 1 shows that the main elements of molybdenum concentrate are Mo and S, and the other main impurity elements are O, Al, K, etc. After high temperature roasting, the main component  $\text{MoS}_2$  in molybdenum concentrate was oxidized to  $\text{MoO}_3$ , which increases the mass ratio of other impurity elements.

In order to further analyze the influence of impurity elements, the advanced mineral liberation analyzer (MLA) was introduced to examine samples from the production process of ammonium molybdate. This technology can quantitatively analyze the form and content of impurity elements, allowing the associations of impurity elements to be identified. Different samples including molybdenum concentrate, molybdenum calcine, water-washed molybdenum calcine, ammonia leaching residue, etc., were analyzed by MLA, among which the analysis results of molybdenum concentrate are shown in Table 2.

**Table 2.** Mineral phase and content of molybdenum concentrate determined by MLA.

Name	Chemical Formula	Percentage of Weight/%	Percentage of Area/%	Area/ $\mu\text{m}^2$	Number of Mineral Particles
Iron	Fe	0.02	0.01	479.27	1
Rutile	$\text{TiO}_2$	0.01	0.01	260.85	3
Calcite	$\text{CaCO}_3$	0.01	0.01	419.36	9
Chlorite	$\text{Fe}^{2+}_3\text{Mg}_{1.5}\text{AlFe}^{3+}_{0.5}\text{Si}_3\text{AlO}_{12}(\text{OH})_6$	0.02	0.04	1092.09	16
Hematite	$\text{Fe}_2\text{O}_3$	0.04	0.03	999.73	18
Kaolinite	$\text{Al}_2\text{Si}_2\text{O}_5(\text{OH})_4$	0.04	0.06	1699.92	16
Illite	$\text{K}_{0.6}(\text{H}_3\text{O})_{0.4}\text{Al}_{1.3}\text{Mg}_{0.3}\text{Fe}^{2+}_{0.1}\text{Si}_{3.5}\text{O}_{10}(\text{OH})$	0.02	0.04	1102.08	18
Fluorite	$\text{CaF}_2$	0.08	0.13	3774.28	19
Orthoclase	$\text{KAlSi}_3\text{O}_8$	0.04	0.07	2045.65	20
Chalcopyrite	$\text{CuFeS}_2$	0.04	0.04	1253.1	20
Anandite	$\text{Ba}_{0.75}\text{K}_{0.25}\text{Fe}^{2+}_{2.25}\text{Mg}_{0.75}\text{Si}_3\text{Al}_{0.7}\text{Fe}^{3+}_{0.5}\text{O}_{10}\text{Si}_{1.5}(\text{OH})_{0.5}$	0.04	0.04	1190.69	26
Minium	$\text{Pb}_2\text{PbO}_4$	0.11	0.07	2020.69	58
Muscovite	$\text{KAl}_3\text{Si}_3\text{O}_{10}(\text{OH})_{1.8}\text{F}_{0.2}$	0.36	0.63	18,799	102
Quartz	$\text{SiO}_2$	0.27	0.51	15,371.7	93
Anhydrite	$\text{CaSO}_4$	0.15	0.25	7366.33	144
Pyrite	$\text{FeS}_2$	1.23	0.21	36,359.88	297
Molybdenite	$\text{MoS}_2$	95.57	85.61	2,554,936.8	25,206
Unknown mineral		1.95	4.81	143,533.6	15,992

It can be seen from Table 2 that in addition to  $\text{MoS}_2$ , sulfur in molybdenum concentrate also exists in the pyrite and chalcopyrite. The potassium minerals in molybdenum concentrate are muscovite, orthoclase, anandite and illite, and the content of muscovite is several times higher than that of the other three minerals. The MLA statistical deviations (confidence degree for 95%) of these four minerals are about 20%, 40%, 60% and 60%. The main iron-containing impurity is pyrite, and the main calcium-containing impurities are anhydrite and fluorite.

### 3.3. Transformation Mechanism of Impurities during Roasting Process

In order to explore the changes in potassium mineralogy during the roasting process, the mineral liberation analyzer was used to conduct phase analysis of each solid phase product from the molybdenum concentrate in the normal production process. The mass fractions of potassium-containing minerals in products from the roasting-washing stages are shown in Figure 5.

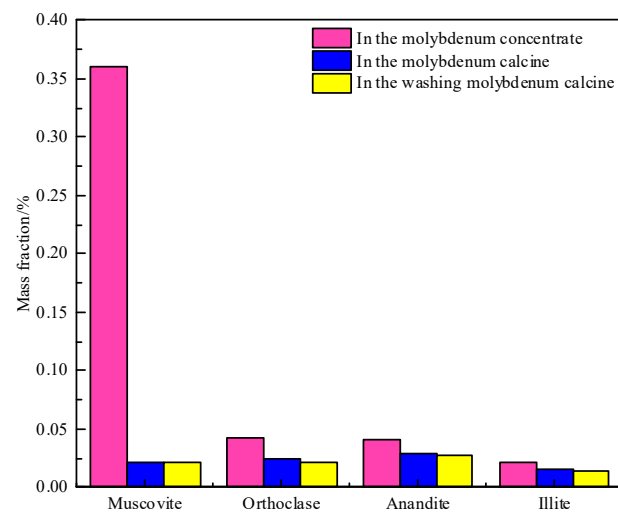


**Figure 5.** Mass fractions of potassium minerals during roasting-washing process.

According to the results in Figure 5, it is necessary to calculate the mass changes of potassium minerals during roasting and washing so that the changes of potassium occurrence forms can be accurately analyzed:

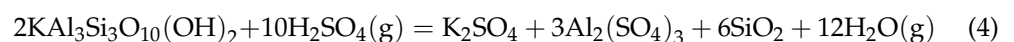
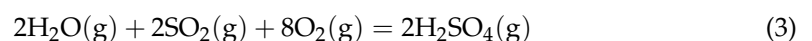
$$M_{i1} = M_1 \cdot \omega_{i1} - M_2 \cdot \omega_{i2} \quad (1)$$

$$M_{i2} = M_2 \cdot \omega_{i2} - M_3 \cdot \omega_{i3} \quad (2)$$

where  $M_{i1}$  is the mass change of a mineral during roasting,  $M_{i2}$  is the mass change of a mineral during washing,  $M_1$  is the mass of molybdenum concentrate,  $M_2$  is the mass of molybdenum calcine in,  $M_3$  is the mass of washed molybdenum calcine in,  $\omega_{i1}$  is the mass fraction of a mineral in molybdenum concentrate,  $\omega_{i2}$  is the mass fraction of a mineral in molybdenum calcine, and  $\omega_{i3}$  is the mass fraction of a mineral in washed molybdenum concentrate.

Since roasting and washing are both processes causing mass loss,  $M_1 > M_2 > M_3$ . As can be seen from Figure 5, the molybdenum concentrate contains muscovite, orthoclase, anandite and illite, and the mass fraction of muscovite and orthoclase decrease obviously after roasting, while the mass fraction of anandite and illite change slightly. According to the study of Tang et al. [20], high-temperature roasting can transform part of insoluble potassium into soluble potassium. Combining with the results calculated from Equation (2), it can be concluded that K-containing minerals are insoluble and not removed by washing, while these minerals could react in the roasting process, so they are the main source of soluble potassium in molybdenum calcine. Additionally, the contents of muscovite and orthoclase change more during roasting. Two minerals are analyzed as examples.

The temperature of roasted molybdenum concentrate is much lower than the melting point of these minerals [28–30]. According to the existing research results [31–36],  $\text{H}_2\text{SO}_4$  promotes the reaction of these K-containing minerals during roasting to destroy the lattice structure, so that potassium and other valuable elements form soluble salts.  $\text{MoS}_2$  is oxidized to generate a large amount of  $\text{SO}_2$  at high temperature. And there may be some crystal  $\text{H}_2\text{O}$  in the minerals and steam in the air. Therefore,  $\text{SO}_2$  reacts with  $\text{O}_2$  and  $\text{H}_2\text{O}$  to form gaseous  $\text{H}_2\text{SO}_4$  during the roasting process of molybdenum concentrate. It is proposed that muscovite and orthoclase react during roasting as follows:



The thermodynamic software Factsage7.0 was used to predict the feasibility of the chemical reaction, and the Gibbs free energy of each reaction at various temperatures was calculated by the following formula:

$$\Delta G_T^\ominus = \Delta H_T^\ominus - T\Delta S_T^\ominus \quad (6)$$

where  $\Delta G_T^\ominus$  is standard molar Gibbs free energy for reaction at various temperatures,  $\text{MJ}\cdot\text{mol}^{-1}$ ;  $\Delta H_T^\ominus$  is standard molar enthalpy of formation for reactions at various temperatures,  $\text{MJ}\cdot\text{mol}^{-1}$ ;  $T$  is thermodynamic temperature for reaction, K;  $\Delta S_T^\ominus$  is standard molar entropy for reactions at various temperatures,  $\text{MJ}\cdot\text{mol}^{-1}\cdot\text{K}^{-1}$ . Thermodynamic analysis of Equations (3)–(5) was carried out by thermodynamic software Factsage7.0, and the functional relationship between  $\Delta G_T^\ominus$  and  $T$  of each reaction in the roasting process was obtained after calculation. The results are as shown in Figure 6.

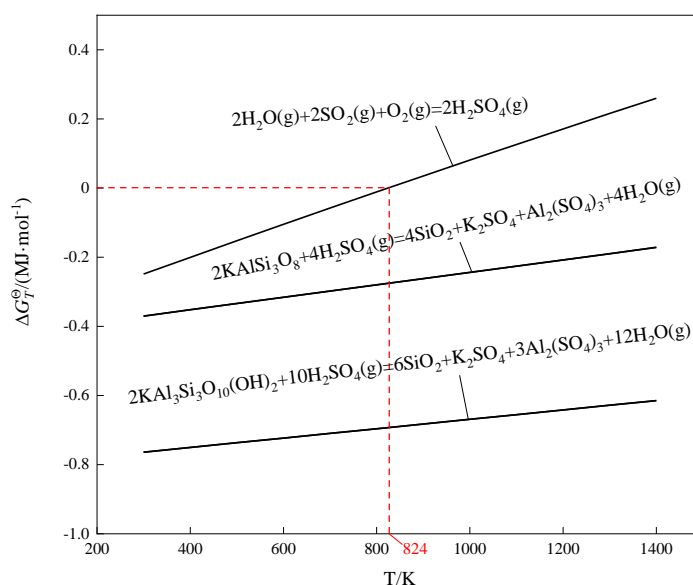


**Figure 6.** Thermodynamic analysis of soluble potassium from orthoclase.

As can be seen from Figure 6, the reaction of Equation (3) can occur spontaneously below 824 K, respectively ( $\Delta G_T^\ominus = 0$ ), so the specific mechanism of producing soluble potassium in roasting process is as follows:

The  $\text{SO}_2$  produced by the oxidation of  $\text{MoS}_2$  can react with  $\text{H}_2\text{O}$  to form gaseous  $\text{H}_2\text{SO}_4$ . The  $\text{K}_2\text{O}$  and  $\text{Al}_2\text{O}_3$  components of muscovite and orthoclase react with  $\text{H}_2\text{SO}_4$  to produce soluble sulfates and release  $\text{SiO}_2$ . Soluble sulfates which are  $\text{Al}_2(\text{SO}_4)_3$  and  $\text{K}_2\text{SO}_4$  can be removed by washing with water. These reactions in reality may only occur to a partial extent.

In order to verify the results of thermodynamic analysis, the contents of  $\text{K}^+$ ,  $\text{Al}^{3+}$  and  $\text{SO}_4^{2-}$  in the washing solution were determined by ICP and IC. The results are shown in the Table 3.

**Table 3.** Ion contents in the washing solution.

Ion Name	Washed Sample	Concentration/( $\text{mmol}\cdot\text{L}^{-1}$ )
$\text{K}^+$	Molybdenite concentrate	0.0317
$\text{K}^+$	Molybdenum calcine	0.2859
$\text{Al}^{3+}$	Molybdenum calcine	0.7297
$\text{SO}_4^{2-}$	Molybdenum calcine	1.1049

It can be seen from Table 3 that soluble potassium is produced in the roasting process of molybdenum concentrate.  $\text{SO}_4^{2-}$  in the washing solution can be determined, and there

is no  $\text{SO}_3^{2-}$  in the washing solution.  $\text{SO}_4^{2-}$  can be coordinated with  $\text{K}^+$  and  $\text{Al}^{3+}$  to form  $\text{K}_2\text{SO}_4$  and  $\text{Al}_2(\text{SO}_4)_3$ . The mole of  $\text{Al}^{3+}$  is slightly below three times that of  $\text{K}^+$ . It indicates that muscovite and orthoclase could be decomposed by  $\text{H}_2\text{SO}_4$  to produce soluble potassium and aluminum salts during roasting. The backscattered electron (BSE) images of the mineral liberation analyzer (MLA) were used to further predict whether muscovite and orthoclase reacted during roasting. The enhanced backscattered electron (BSE) images of muscovite and orthoclase in molybdenum concentrate, molybdenum calcine, and washed molybdenum calcine are shown in Figure 7.

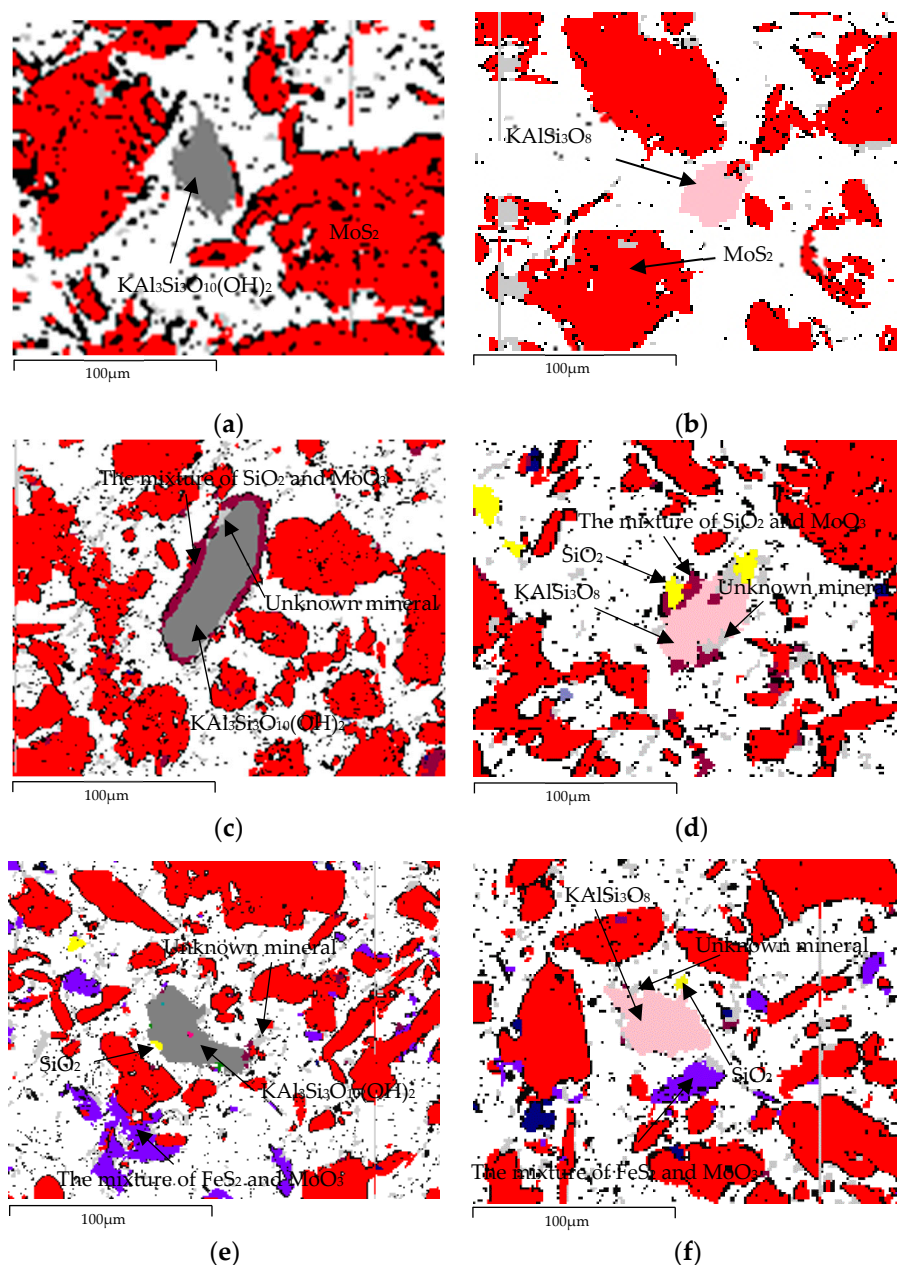


**Figure 7.** Enhanced backscattered electron microscope images of molybdenum concentrate, molybdenum calcine and washed molybdenum calcine. (a) Muscovite in molybdenum concentrate; (b) Orthoclase in molybdenum concentrate; (c) Muscovite in molybdenum calcine; (d) Orthoclase in molybdenum calcine; (e) Muscovite in washed molybdenum calcine (f) Orthoclase in washed molybdenum calcine.

As shown in Figure 7a,b, there are no other substances or minerals around muscovite and orthoclase in molybdenum concentrate before roasting. However, after roasting, all

muscovite and orthoclase are surrounded by mixtures of  $\text{MoO}_3$  and  $\text{SiO}_2$  in molybdenum calcine, and each example is shown in Figure 7c,d. Hence, these seemed to have partially reacted to generate  $\text{SiO}_2$  during roasting. Furthermore, there are some unknown minerals on the surface; one of which could be arcanite ( $\text{K}_2\text{SO}_4$ ). Most of these minerals can be removed after washing as shown Figure 7e,f. Therefore, it can be concluded that the unknown minerals are  $\text{K}_2\text{SO}_4$  and  $\text{Al}_2(\text{SO}_4)_3$  generated by the reaction of the muscovite and orthoclase with gases during roasting leaving residual  $\text{SiO}_2$ . Thus, the specific reactions for producing soluble potassium in roasting process can be verified.

### 3.4. Effect of Humidification on the Removal of Impurity Elements

In order to further verify the mechanism proposed in Section 3.3 and to put forward effective suggestions for removing impurity elements, the experiment on humidification of molybdenum concentrate during roasting was carried out. It has been known that molybdenum concentrate begins to oxidize at  $450^\circ\text{C}$  and rapidly oxidizes above  $500^\circ\text{C}$  [28]. Half an hour before the end of the roasting, the roasting temperature was set to  $500^\circ\text{C}$ , and water vapor and air were mixed in a ratio of 1:2 and passed into the tube furnace. After the humidification and roasting, the cooled samples were washed with water three times. The washed samples were then analyzed by XRF and MLA, respectively, and compared with the normal non-humidified samples as shown in Tables 4 and 5.

**Table 4.** Effect of humidification on the content of impurity elements in washed molybdenum calcine/%.

Element	Al	K	S	Si	Fe	Mo	Ca
Humidified	0.09	0.12	1.06	1.09	0.98	56.4	0.23
Non-humidified	0.14	0.15	1.08	1.12	1.04	56.7	0.25

**Table 5.** MLA analysis results of washed molybdenum calcine under different conditions/%.

Name	Chemical Formula	Percentage of Weight/% (Humidified)	Percentage of Weight/% (Non-Humidified)
Molybdenum Oxide	$\text{MoO}_3$	86.43	86.80
Orthoclase	$\text{KAlSi}_3\text{O}_8$	0.03	0.17
Rutile	$\text{TiO}_2$	0.01	0.01
Corundum	$\text{Al}_2\text{O}_3$	0.38	0.52
Hematite	$\text{Fe}_2\text{O}_3$	0.29	0.48
Ferrotschermakite	$\text{Ca}_2\text{MgFe}_2\text{Al}_3\text{FeSi}_6\text{O}_{22}(\text{OH})_2$	0.01	0.07
Illite	$\text{K}_{0.6}(\text{H}_3\text{O})0.4\text{Al}_{1.3}\text{Mg}_{0.3}\text{Fe}^{2+}_{0.1}\text{Si}_{3.5}\text{O}_{10}(\text{OH})$	0.01	0.02
Fluorite	$\text{CaF}_2$	0.07	0.09
Ferrimolybdate	$\text{Fe}^{3+}_2(\text{MoO}_4)_3 \cdot n(\text{H}_2\text{O})$	0.75	1.11
Anandite	$\text{Ba}_{0.75}\text{K}_{0.25}\text{Fe}^{2+}_{2.25}\text{Mg}_{0.75}\text{Si}_3\text{Al}_{0.7}\text{Fe}^{3+}_{0.3}\text{O}_{10}\text{S}_{1.5}(\text{OH})_{0.5}$	0.44	0.46
Muscovite	$\text{KAl}_3\text{Si}_3\text{O}_{10}(\text{OH})_{1.8}\text{F}_{0.2}$	0.05	0.10
Quartz	$\text{SiO}_2$	1.12	1.67
Molybdenite	$\text{MoS}_2$	0.03	0.02
Mixture of molybdenum oxide and pyrite	$\text{MoO}_3, \text{FeS}_2$	1.81	1.61
Mixture of molybdenum oxide and anhydrite	$\text{MoO}_3, \text{CaSO}_4$	0.95	0.83
Mixture of molybdenum oxide and quartz	$\text{MoO}_3, \text{SiO}_2$	1.66	1.53
Mixture of quartz and pyrite	$\text{SiO}_2, \text{FeS}_2$	0.37	0.31

It can be seen from Table 4 that the contents of impurity elements Al and K in the humidified sample have decreased significantly compared with the normal non-humidified sample, which indicates that humidification may increase the conversion of impurity minerals to soluble ions. To further explain the mechanism of humidification, advanced MLA was again used to quantitatively analyze impurity minerals in different samples as shown in Figure 8 and Table 5.

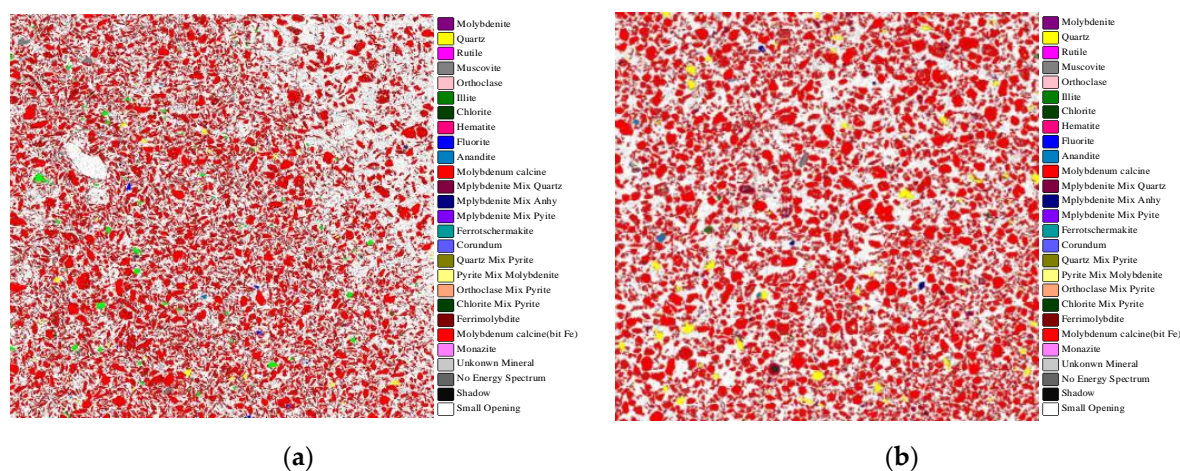


**Figure 8.** MLA scan analysis images under different conditions. (a) MLA scan analysis image of humidified molybdenum calcine; (b) MLA scan analysis image of Non-humidified molybdenum calcine.

It can be seen from the results in Table 5 that the orthoclase content of the humidified sample is 0.03%, which is significantly lower than that of the normal sample without humidification (0.17%). The main reason is that the humidification can facilitate more of the  $\text{SO}_2$  oxidized from molybdenum concentrate adhering to the surface of molybdenum concentrate particles in the form of  $\text{H}_2\text{SO}_4$ . Combined with the analysis results in Section 3.3, most of the impurity elements in molybdenum concentrate exist in the form of alkaline minerals or compounds. Therefore, the reaction degree of Equations (4) and (5) increases due to the increase of  $\text{H}_2\text{SO}_4$  content, that is, more alkaline minerals are converted into soluble ions at high temperature, and then removed by water washing, resulting in a reduced content of impurity elements. Therefore, the conversion of alkaline mineral impurities to soluble ions can be increased by humidifying, which is beneficial to the production under the current water washing process conditions. In addition, it can be seen from Table 5 that different sintering mixtures such as the mixture of  $\text{MoO}_3$  and  $\text{FeS}_2$ , the mixture of  $\text{MoO}_3$  and  $\text{CaSO}_4$ , etc., were formed after roasting. This is consistent with Wang et al.'s research [25].

### 3.5. Influence Mechanism of Impurities on Molybdenum Leaching

The phases of the ammonia leaching residue in Section 2.2 were analyzed by XRD, and the results are shown in Figure 9.

After ammonia leaching, there is still molybdenum in the solid phase, which cannot be extracted into the ammonium molybdate solution, resulting in the loss of molybdenum. XRD results show that the main minerals in ammonia leaching residue are  $\text{MoO}_3$ ,  $\text{SiO}_2$ ,  $\text{CaSO}_4$ ,  $\text{FeS}_2$ , orthoclase and muscovite, among which the content of  $\text{MoO}_3$  is relatively high. In order to further analyze the reasons affecting the Mo extraction, the mineral liberation analyzer (MLA) was used for the quantitative analysis of the phase composition of ammonia leaching residue, and different forms and contents of molybdenum in ammonia leaching residue were obtained, as shown in Figures 10 and 11.

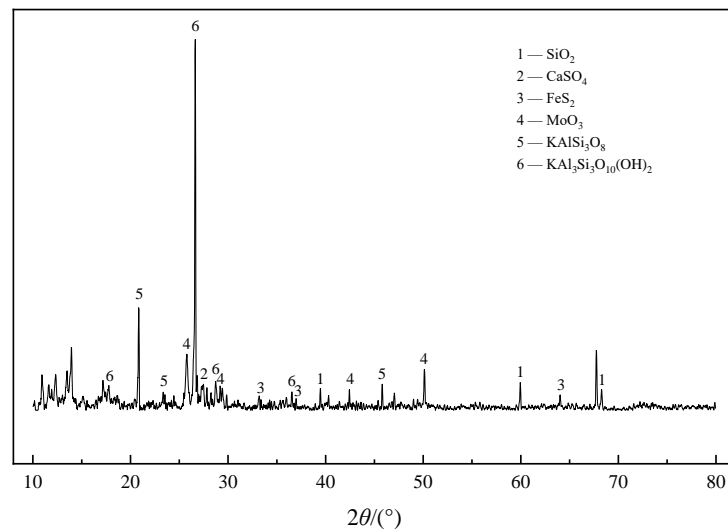


Figure 9. XRD analysis of ammonia leaching residue.

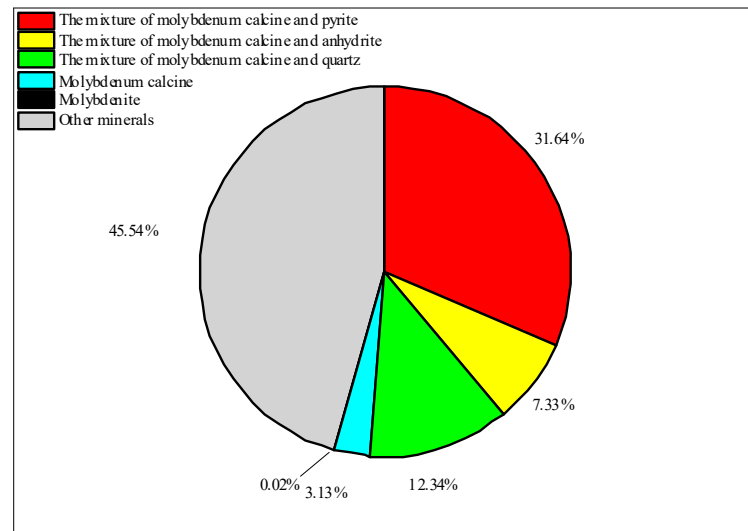


Figure 10. The existence form of molybdenum in ammonia leaching residue/%.

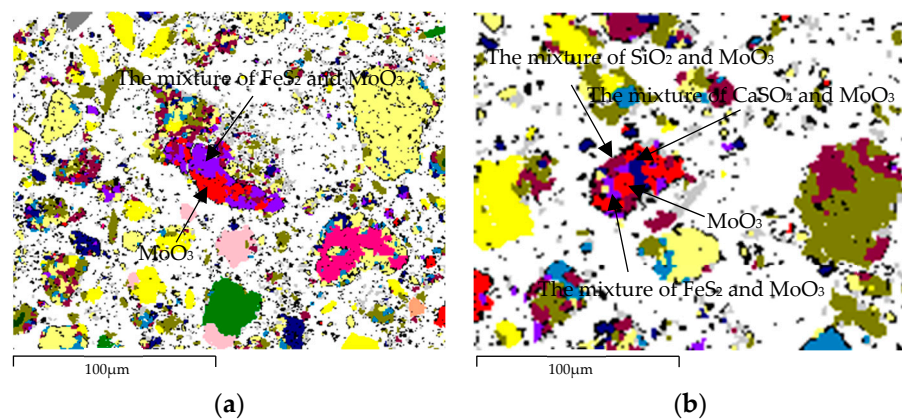


Figure 11. Enhanced backscattered electron microscope images of mixtures and MoO<sub>3</sub> in ammonia leaching residue. (a) position 1; (b) position 2.

It can be seen from Figures 10 and 11 that MoO<sub>3</sub> in ammonia leaching residue mostly exists in the mixtures formed with FeS<sub>2</sub>, CaSO<sub>4</sub> and SiO<sub>2</sub>. It has been known that pyrite

is present in the concentrate. It is unclear how much  $\text{CaF}_2$  reacts during roasting to form  $\text{CaSO}_4$ . Additionally, we cannot be certain how much of the  $\text{SiO}_2$  encapsulation is due to quartz or formed from the reaction of K-containing minerals. The content of  $\text{MoO}_3$  alone is low (3.13%), and the unoxidized  $\text{MoS}_2$  only accounts for 0.02%. In addition, the proportions of the mixture of  $\text{MoO}_3$  and  $\text{FeS}_2$ ,  $\text{CaSO}_4$ ,  $\text{SiO}_2$  accounted for 31.6%, 7.33%, 12.3%, respectively. This indicates that the impurities  $\text{FeS}_2$ ,  $\text{CaSO}_4$  and  $\text{SiO}_2$  encapsulates  $\text{MoO}_3$  and hinders the leaching of Mo, especially  $\text{FeS}_2$  which has the greatest influence on the leaching of Mo.

Through the detection and analysis of the mineral liberation analyzer (MLA) as shown in Table 5, it was found that the mixture containing  $\text{MoO}_3$  was formed in the process of high-temperature roasting. According to the analysis results in Section 3.3, the specific mechanism can be concluded as follows:

The main calcium substances in molybdenum concentrate are  $\text{CaSO}_4$  and  $\text{CaF}_2$ . As the temperature reached 673 K,  $\text{MoS}_2$  was oxidized to generate  $\text{MoO}_3$ , which is an exothermic reaction. A large amount of exothermic reaction increases the local surface temperature, leading to the appearance of molten  $\text{MoO}_3$  [37]. The released  $\text{SO}_2$  and  $\text{O}_2$  could convert  $\text{CaF}_2$  into  $\text{CaSO}_4$ , which is an endothermic reaction. Therefore, a large amount of  $\text{CaSO}_4$  contacted with the surrounding molten  $\text{MoO}_3$  and formed a mixture after cooling. Part of the  $\text{MoO}_3$  encapsulated in the interior is not easy to extract in the ammonia leaching process.

As the oxidation of  $\text{FeS}_2$  begins slowly at least above 673 K [38–40], the alkaline oxides such as  $\text{FeO}$ ,  $\text{Fe}_3\text{O}_4$  and  $\text{Fe}_2\text{O}_3$  which produce a thin layer on the surface of  $\text{FeS}_2$  can undergo solid phase reaction with  $\text{MoO}_3$ , and the generated sintered phase firmly connects  $\text{FeS}_2$  and  $\text{MoO}_3$  [25]. The remaining  $\text{FeS}_2$  was encapsulated inside the particle before oxidation, preventing the contact between  $\text{FeS}_2$  and  $\text{O}_2$ , and explaining the formation of a mixture of  $\text{FeS}_2$  and  $\text{MoO}_3$ . In addition, during the roasting process,  $\text{SiO}_2$  will also come into contact with locally melted  $\text{MoO}_3$  at high temperature and form dense sintered particles after cooling, so that the  $\text{MoO}_3$  encapsulated in the sinter cannot be leached.

In summary, impurities such as  $\text{CaSO}_4$ ,  $\text{FeS}_2$  and  $\text{SiO}_2$  will be sintered with  $\text{MoO}_3$  in the roasting process. Then a solid sinter will be formed to encapsulate a portion of the  $\text{MoO}_3$ , which will hinder the leaching of  $\text{MoO}_3$ , thus reducing the extraction of Mo.

### 3.6. Effect of Particle Size on Leaching of Molybdenum and Potassium

The changes of mass fractions of Mo and K in samples with different particle sizes in the production process were obtained by the experimental method of Section 2.2. The X-ray fluorescence spectrometry (XRF) test results were verified by ICP test results, and the X-ray fluorescence spectrometry (XRF) test results were shown in Figure 12.

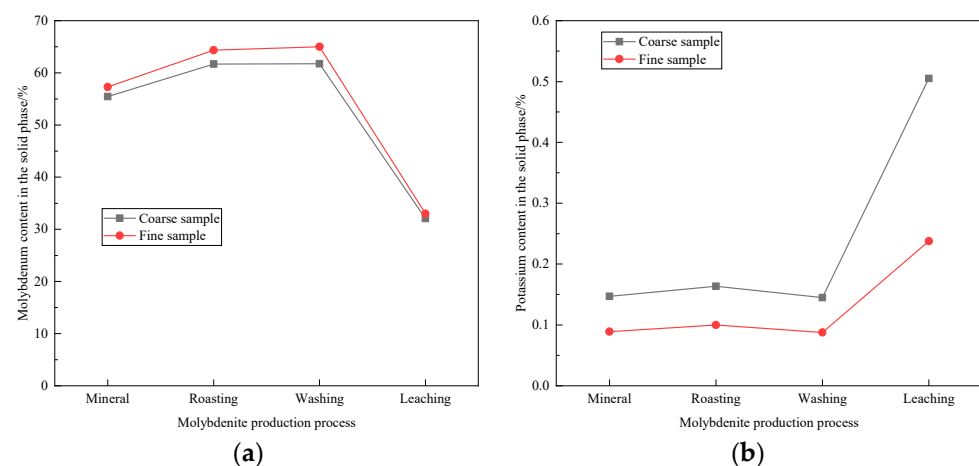


**Figure 12.** Variation of element content in samples with different particle sizes. (a) Mass fraction change of Mo; (b) mass fraction change of K.

According to the test results in Figure 12, the change of element mass in each process is calculated respectively so that the influence of potassium and molybdenum content in samples with different particle sizes during roasting, washing and ammonia leaching is accurately analyzed:

$$m_{i1} = m_1 \cdot \omega_{i1}' - m_1' \cdot \omega_{i2}' \quad (7)$$

$$m_{i2} = m_2 \cdot \omega_{i2}' - m_2' \cdot \omega_{i3}' \quad (8)$$

$$m_{i3} = m_3 \cdot \omega_{i3}' - m_3' \cdot \omega_{i4}' \quad (9)$$

where  $m_{i1}$ ,  $m_{i2}$  and  $m_{i3}$  are the mass loss of an element during roasting, water washing and ammonia leaching respectively, g;  $m_1$  and  $m_1'$  are, respectively, the mass of samples before and after roasting in Section 2.1, g;  $m_2$  and  $m_2'$  are, respectively, the mass of sample before and after washing in Section 2.1, g;  $m_3$  and  $m_3'$  are, respectively, the mass of sample before and after ammonia leaching in Section 2.1, g;  $\omega_{i1}'$ ,  $\omega_{i2}'$ ,  $\omega_{i3}'$  and  $\omega_{i4}'$  are the mass fractions of an element in the samples before roasting, after roasting, after washing and after ammonia leaching, respectively.

According to the results of Figure 12 and the calculation of Equations (7) and (8), Mo has little mass loss during roasting and washing. The mass loss of K in the roasting process is very small, but the mass loss in the washing process is very large, mainly because soluble  $K^+$  is removed in the washing process.

Using the data from Figure 12 and calculations using Equation (9), the change in solid phase masses of Mo and K that are during the ammonia leaching process can be calculated. In order to fully express the extraction efficiency of molybdenum and potassium for the two samples in the ammonia leaching process, 10 g each of washed molybdenum calcine were taken for ammonia leaching, and mass changes of the solids, and contents of Mo and K were calculated and shown in Figure 13.

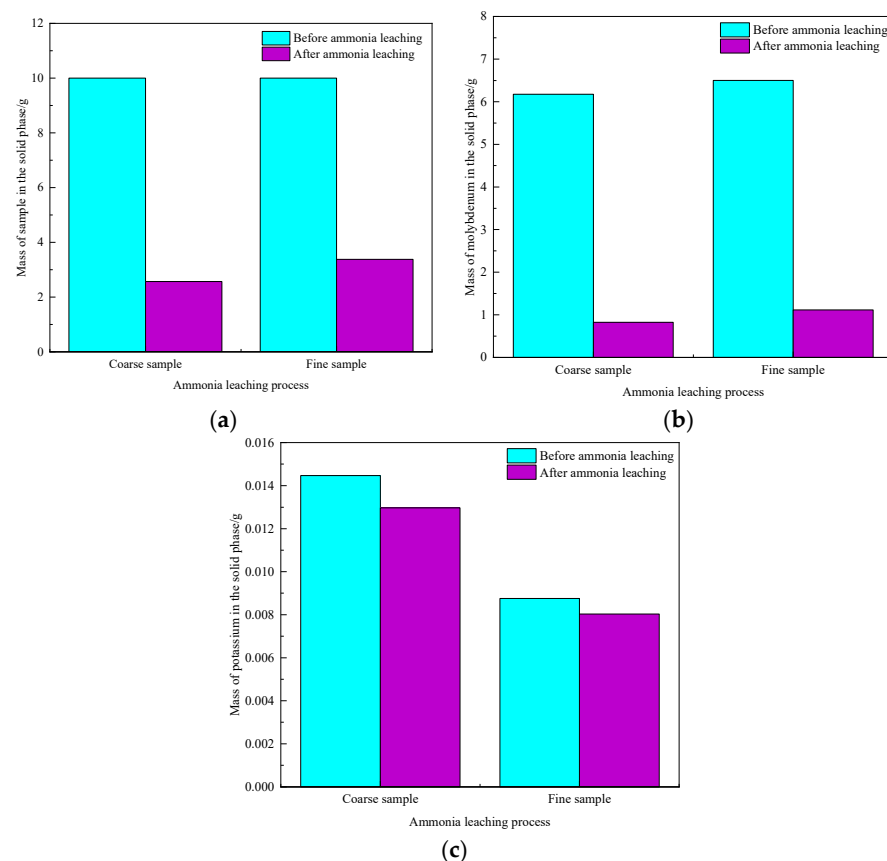


**Figure 13.** Mass change of elements in samples with different particle sizes during ammonia leaching. (a) Mass change of sample, (b) mass change of Mo, (c) mass change of K.

As shown in Figure 13, elements in the coarse sample are more conducive to extracting into ammonia solution. The extraction of molybdenum in the fine samples is slightly higher than that in the coarse sample. Potassium in the fine sample is more difficult to extract into ammonia solution. Therefore, the particle size of the molybdenum concentrate sample has noticeable impact on the extraction of molybdenum and potassium. The extractions can be calculated by the following formula:

$$\mu_i = \frac{m_3 \cdot \omega_{i3}' - m_3' \cdot \omega_{i4}'}{m_3 \cdot \omega_{i3}'} \cdot 100\% \quad (10)$$

where  $\mu_i$  is the extraction of an element in the sample during ammonia leaching, %. The extractions of molybdenum and potassium are 86.7% and 10.3%, respectively, in the coarse sample, and 82.8% and 8.35% respectively in the fine sample.

Production experience shows that molybdenum concentrate roasting is usually accompanied by sintering. After roasting and washing, most  $\text{MoO}_3$  can be leached into ammonia leaching solution, while the remaining small amount of  $\text{MoO}_3$  is not contacted by ammonia water because it forms the three mixtures analyzed in Section 3.5 with impurities during roasting (as shown in Figure 11). Based on the properties and characteristics of the products formed after roasting of molybdenum concentrate with different particle sizes in the above simulation experiment, and verified by the analysis of microstructure solid phase structure of BSE, the influence mechanism of sintered particles which forms from molybdenum concentrate with different particle sizes during roasting on the ammonia leaching effect can be obtained, and its schematic diagram is shown in Figure 14.

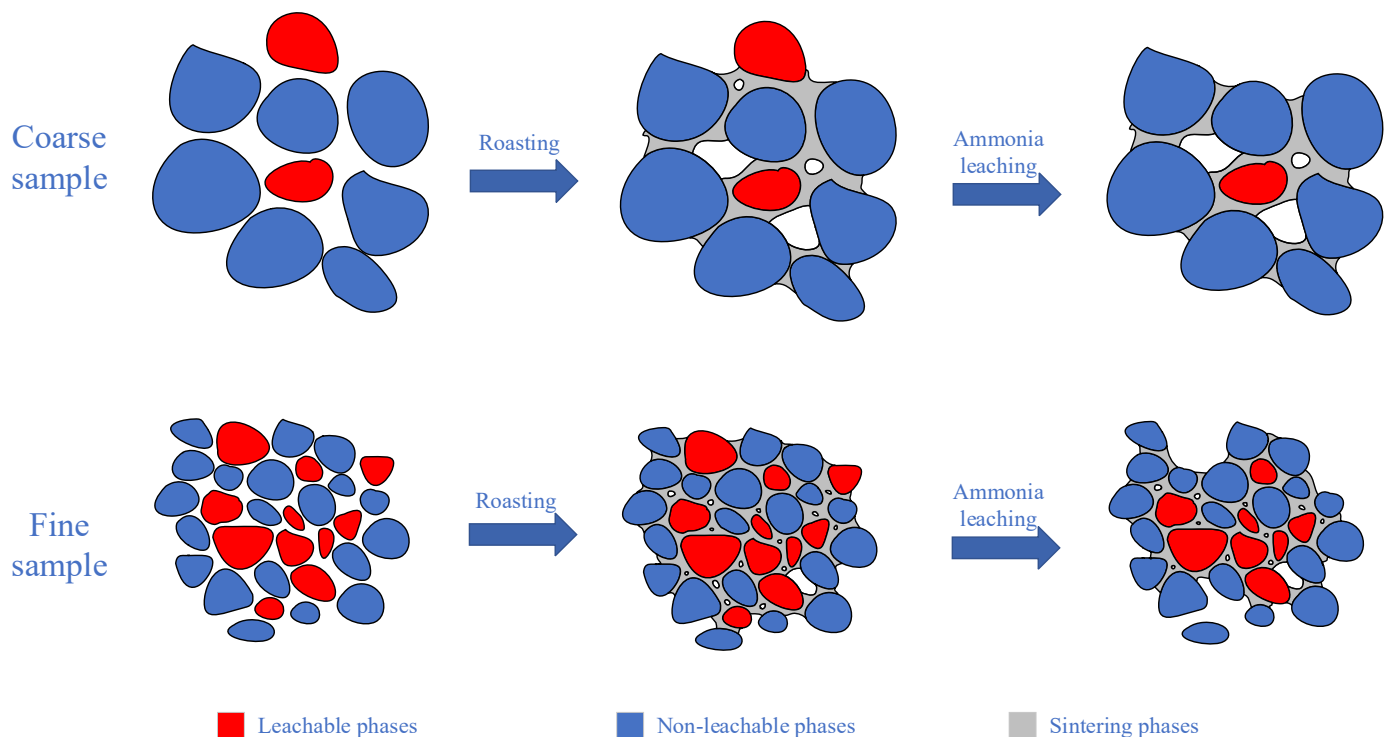


**Figure 14.** Leaching mechanism of phases in samples with different particle sizes during ammonia leaching process.

As can be seen from Figure 14, sintering necks can be formed between some adjacent substances, and part of  $\text{MoO}_3$  and K-containing minerals are encapsulated in the particles and cannot contact with the liquid phase. Compared with coarse particle size molybdenum concentrate, the sintered products generated by fine particle size molybdenum concentrate have higher density and smaller pore area. This reduces the contact area between the leachable components and ammonia water, thereby reducing the extractions of Mo and K.

#### 4. Conclusions

(1) Typical impurity elements are mainly present in molybdenum concentrates in the form of large molecular weight potassium minerals and other minerals that include  $\text{FeS}_2$ ,  $\text{CaSO}_4$ ,  $\text{SiO}_2$ , etc.  $\text{FeS}_2$ ,  $\text{CaSO}_4$ ,  $\text{SiO}_2$  and other impurities significantly promoted the formation of sintered aggregates during roasting process, and the sintered aggregates further hindered the extraction of Mo and K. Humidification during roasting was conducive to improving the conversion of impurity silicate minerals to soluble ions. Roasting fine molybdenum concentrate was helpful to reduce the impurity content in molybdenum products.

(2) The results of experimental and thermodynamic analysis show that K in molybdenum concentrate mainly comes from muscovite and orthoclase. During the roasting process, the  $\text{H}_2\text{SO}_4$  formed by the contact between the water formed by the dehydration of minerals and the roasted gas product  $\text{SO}_2$  can promote the transformation of potassium minerals into soluble ions. Therefore, the amount of  $\text{H}_2\text{SO}_4$  generated on the particle surface can be increased by increasing the dehydration rate of minerals or humidification, thus increasing the conversion of impurity minerals to soluble ions. This is conducive to improving the purity of ammonium molybdate products.

(3) The particle size of molybdenum concentrate impacts the extraction of Mo and K. Compared with coarse molybdenum concentrate, fine molybdenum concentrate was easier to form compact sintered particles with impurities such as  $\text{FeS}_2$ ,  $\text{CaSO}_4$ ,  $\text{SiO}_2$ .  $\text{MoO}_3$  is encapsulated in the sintered agglomerates and cannot contact with ammonia water, hence only  $\text{MoO}_3$  on the outside of the sintered agglomerates can be dissolved in ammonia water, thus reducing the extraction of Mo.

**Author Contributions:** Conceptualization, Q.L. and W.F.; methodology, Q.L.; resources, Q.L.; software, R.L.; formal analysis, Q.L. and R.L.; investigation, R.L. and M.W.; data curation, R.L. and S.Y.; writing, Q.L. and R.L.; writing—review and editing, Q.L. and R.L.; supervision, Q.L. and S.Y.; project administration, Q.L. and S.Y.; funding acquisition, Q.L. All authors have read and agreed to the published version of the manuscript.

**Funding:** The authors would like to express their thanks for the support to this work by Natural Science Foundation of Shaanxi Province (2019JLM-34).

**Data Availability Statement:** Not applicable.

**Conflicts of Interest:** The authors declare no conflict of interest.

#### References

1. Zhong, C.H.; Wang, H.H.; Zhang, L.Z.; Guo, M.C.; Feng, B. Flotation separation of molybdenite and talc by xanthan gum. *Powder Technol.* **2021**, *388*, 158–165. [[CrossRef](#)]
2. Sheybani, K.; Paydar, M.H.; Shariat, M.H. Effect of mechanical activation on aluminothermic reduction of molybdenum trioxide. *Int. J. Refract. Hard Met.* **2019**, *82*, 245–254. [[CrossRef](#)]
3. Shafiei Bafti, B.; Svojtka, M.; Abdolahi, M. Geochemistry of Rhenium and Other Trace Elements in Molybdenite; SarCheshmeh Porphyry Cu-Mo Deposit, Iran. *Acta Geol. Sin. Engl.* **2021**, *95*, 19. [[CrossRef](#)]
4. Gan, M.; Fan, X.; Chen, X.; Wu, C. Reaction mechanisms of low-grade molybdenum concentrate during calcification roasting process. *Trans. Nonferrous Met. Soc. China* **2016**, *26*, 3015–3023. [[CrossRef](#)]
5. Tyagi, P.; Choudhary, S. Tuning the electronic and optical properties of molybdenite ( $\text{MoS}_2$ ) by adsorption of alkali metals and halogens. *Opt. Mater.* **2021**, *118*, 111248.1–111248.8. [[CrossRef](#)]
6. Keilholz, S.; Kohlmann, H.; Uhlenhut, H.; Gabke, A.; Garcia-Schollenbruch, M. In situ X-ray diffraction studies on the production process of molybdenum. *Inorg. Chem.* **2022**, *61*, 10126–10132. [[CrossRef](#)]
7. Zhu, Q.; Xie, M.X.; Shang, X.T.; An, G.; Sun, J.; Wang, N.; Xi, S.; Bu, C.Y.; Zhang, J.P. Research Status and Progress of Welding Technologies for Molybdenum and Molybdenum Alloys. *Metals* **2020**, *10*, 279. [[CrossRef](#)]
8. Gui, D.; Hua, Y.N.; Xing, Z.X.; Zhao, S.P. Investigation of Potassium Contamination in SOI Wafer Using Dynamic SIMS. *IEEE Trans. Device Mater. Reliab.* **2007**, *7*, 369–372. [[CrossRef](#)]
9. Hung, H.Y.; Lu, C.W.; Lee, C.Y.; Hsu, C.S.; Hsieh, Y.Z. Analysis of metal ion impurities in liquid crystals using high resolution inductively coupled plasma mass spectrometry. *Anal. Methods* **2012**, *4*, 3631–3637. [[CrossRef](#)]
10. Shekhter, L.N.; Litz, J.E.; Shan, N.M.; Mchugh, L.F. Thermodynamic modelling of molybdenite roasting in a multiple-hearth furnace. *JOM* **2021**, *73*, 873–880. [[CrossRef](#)]

11. Kan, S.; Benzeik, K.; Odabas, Ö.C.; Yvcel, O. Investigation of molybdenite Concentrate Roasting in Chamber and Rotary Furnaces. *Min. Met. Explor.* **2021**, *38*, 1597–1608. [[CrossRef](#)]
12. Chen, Y.; Xie, J.; Chang, Q.; Ma, D. Research progress of preparation technology of molybdenum powder. *Trans. Mater. Heat Treat.* **2020**, *41*, 14–24. (In Chinese)
13. Zhang, M.P.; Liu, C.H.; Zhu, X.J.; Xiong, H.B.; Zhang, L.B.; Gao, J.Y.; Liu, M.H. Preparation of ammonium molybdate by oxidation roasting of molybdenum concentrate: A comparison of microwave roasting and conventional roasting. *Chem. Eng. Process* **2021**, *167*, 108550. [[CrossRef](#)]
14. Liu, J.; Qiu, Z.F.; Yang, J.; Cao, L.M.; Zhang, W. Recovery of Mo and Ni from spent acrylonitrile catalysts using an oxidation leaching–chemical precipitation technique. *Hydrometallurgy* **2016**, *164*, 64–70. [[CrossRef](#)]
15. Li, X.Y.; Zhang, L.; Wang, G.H.; Qin, M.L.; Qu, X.H.; So, K.P. Influence of impurities on hot-rolled molybdenum for high temperature applications. *Int. J. Refract. Met. Hard Mater.* **2020**, *92*, 105294. [[CrossRef](#)]
16. Cheng, L.; Zhao, Z.; Zhao, Y.; Ding, W.; Zhang, Y.; Huang, W. Preparation of high purity molybdenum disulfide by one stage purification from molybdenum concentrate. *Chem. Eng.* **2018**, *32*, 11–13. (In Chinese)
17. Gao, Z.; Xie, X.; Hui, S. New method for producing impurity of molybdenum disulfide. *China Molybdenum Ind.* **2019**, *43*, 42–45. (In Chinese)
18. Aracena, A.; Sanino, A.; Jerez, O. Dissolution kinetics of molybdenite in KOH media at different temperatures. *Trans. Nonferrous Met. Soc. China* **2018**, *28*, 177–185. [[CrossRef](#)]
19. Yang, L.Q.; Li, X.B.; Qi, T.G.; Liu, G.H.; Peng, Z.H.; Zhou, Q.S. Direct synthesis of pure ammonium molybdates from ammonium tetramolybdate and ammonium bicarbonate. *ACS Sustain. Chem. Eng.* **2020**, *8*, 18237–18244. [[CrossRef](#)]
20. Tang, L.; Li, X.; Liu, D. Soluble potassium change mechanism analysis in the process of roasting molybdenum concentrate mineral. *China Molybdenum Ind.* **2016**, *40*, 42–43+49. (In Chinese)
21. Yi, G.S.; Macha, E.; Dyke, J.V.; Macha, R.; McKay, T.; Free, M.L. Recent progress on research of molybdenite flotation: A review. *Adv. Colloid Interface Sci.* **2021**, *295*, 102466. [[CrossRef](#)] [[PubMed](#)]
22. Shalchian, H.; Khaki, J.V.; Babakhani, A.; Michelis, I.D.; Veglio, F.; Parizi, M.T. An enhanced dissolution rate of molybdenite and variable activation energy. *Hydrometallurgy* **2018**, *175*, 52–63. [[CrossRef](#)]
23. Wang, L.; Zhang, G.H.; Dang, J.; Chou, K.C. Oxidation roasting of molybdenite concentrate. *Trans. Nonferrous Met. Soc. China* **2015**, *25*, 4167–4174. [[CrossRef](#)]
24. Tumen-Ulzii, N.; Batnasan, A.; Gunchin, B. Selective dissolution of copper and iron from molybdenite concentrate using acidic sodium nitrate solution. *Miner. Eng.* **2022**, *185*, 107715. [[CrossRef](#)]
25. Wang, L.; Zhang, G.H.; Wang, J.S.; Chou, K.C. Influences of different components on agglomeration behavior of MoS<sub>2</sub> during oxidation roasting process in air. *Metall. Mater. Trans. B* **2016**, *47*, 2421–2432. [[CrossRef](#)]
26. Popov, V.V.; Menushenkov, A.P.; Yastrebtev, A.A.; Molokova, A.Y.; Pisarev, A.A.; Khramov, E.V.; Zubavichus, Y.V.; Shchetinin, I.V.; Ponkratov, K.V.; Tsarenko, N.A.; et al. The synthesis and studies of crystal/local structures and morphology of hydrated molybdenum oxides. *J. Solid State Chem.* **2021**, *301*, 122356. [[CrossRef](#)]
27. Camalan, M.; Cavur, M. Development of a supervised classification method to construct 2D mineral maps on backscattered electron images. *Turk. J. Electr. Eng. Comput. Sci.* **2019**, *28*, 1030–1043. [[CrossRef](#)]
28. Li, X.B.; Wu, T.; Zhou, Q.S.; Qi, T.G.; Peng, Z.H.; Liu, G.H. Kinetics of oxidation roasting of molybdenite with different particle sizes. *Trans. Nonferrous Met. Soc. China* **2021**, *31*, 842–852. [[CrossRef](#)]
29. Lv, L.; Li, C.; Zhang, G.H.; Hu, X.W.; Liang, B. Decomposition behavior of CaSO<sub>4</sub> during potassium extraction from a potash feldspar-CaSO<sub>4</sub> binary system by calcination. *Chin. J. Chem. Eng.* **2018**, *26*, 838–844. [[CrossRef](#)]
30. Massonne, H.J.; Fockenber, T. Melting of phengite-bearing eclogite at pressures of 4 and 9 GPa relevant to deep regions of a subduction zone. *Earth Planet. Sci. Lett.* **2022**, *584*, 117475. [[CrossRef](#)]
31. Jena, S.K.; Mohanty, B.; Padhy, G.; Sahu, J.; Kandi, S.K. Potassium recovery from muscovite using NaCl-roasting followed by H<sub>2</sub>SO<sub>4</sub>-leaching. *J. Cent. South Univ.* **2022**, *29*, 1881–1894. [[CrossRef](#)]
32. Yuan, J.Y.; Yang, J.; Ma, H.W.; Su, S.Q.; Chang, Q.Q.; Komarneni, S. Hydrothermal Synthesis of nano-kaolinite from K-feldspar. *Ceram. Int.* **2018**, *44*, 15611–15617. [[CrossRef](#)]
33. Salimkhani, H.; Joodi, T.; Bordbar-Khiabani, A.; Dizaji, A.M.; Abdolalipour, B.; Azizi, A. Surface and structure characteristics of commercial K-Feldspar powders: Effects of temperature and leaching media. *Chin. J. Chem. Eng.* **2020**, *28*, 307–317. [[CrossRef](#)]
34. Liu, C.J.; Ma, H.W. Hydrothermal decomposition process of K-feldspar in NaOH solution. *Asia-Pac. J. Chem. Eng.* **2020**, *16*, e2578. [[CrossRef](#)]
35. Liu, J.N.; Zhai, Y.C.; Wu, Y.; Zhang, J.; Shen, X.Y. Kinetics of roasting potash feldspar in presence of sodium carbonate. *J. Cent. South Univ.* **2017**, *24*, 1544–1550. [[CrossRef](#)]
36. Ma, J.Y.; Zhang, Y.F.; Qin, Y.H.; Wu, Z.K.; Wang, T.L.; Wang, C.W. The leaching kinetics of K-feldspar in sulfuric acid with the aid of ultrasound. *Ultrason. Sonochem.* **2017**, *35*, 304–312. [[CrossRef](#)]
37. Wang, L.; Li, M.; Que, B.; Xue, Z.; Zhang, G.; Lan, W. Oxidation roasting of molybdenite concentrate. *Chin. J. Nonferr. Metal.* **2021**, *31*, 1952–1964. (In Chinese) [[CrossRef](#)]
38. Gomes, T.; Rosa, R.; Cargnin, M.; Quadri, M.B.; Peterson, M.; Oliveira, C.M.; RosaRabelo, N.; Angioletto, E. Pyrite roasting in modified fluidized bed: Experimental and modeling analysis. *Chem. Eng. Sci.* **2022**, *261*, 117977. [[CrossRef](#)]

39. Aracena, A.; Jerez, O.; Ortiz, R.; Morales, J. Pyrite oxidation kinetics in an oxygen–nitrogen atmosphere at temperatures from 400 to 500 °C. *Can. Metall. Q.* **2016**, *55*, 195–201. [[CrossRef](#)]
40. Zhang, Y.; Li, Q.; Liu, X.L.; Xu, B.; Yang, Y.B.; Jiang, T. A Thermodynamic Analysis on the Roasting of Pyrite. *Minerals* **2019**, *9*, 220. [[CrossRef](#)]

**Disclaimer/Publisher’s Note:** The statements, opinions and data contained in all publications are solely those of the individual author(s) and contributor(s) and not of MDPI and/or the editor(s). MDPI and/or the editor(s) disclaim responsibility for any injury to people or property resulting from any ideas, methods, instructions or products referred to in the content.